CrossMark

ORIGINAL ARTICLE

Detecting transition to chatter mode in peakless tool turning by monitoring vibration and acoustic emission signals

A. V. Filippov[1,2] · V. E. Rubtsov[1] · S. Yu. Tarasov[1,2] · O. A. Podgornykh[2] ·
N. N. Shamarin[2]

Abstract Stability of a peakless tool turning on slender shafts was studied under conditions of low- and high-magnitude vibrations by registering and short-time Fourier transformation (STFT) processing of acoustic emission (AE) and vibration acceleration (VA) signals. Both VA and AE signals have been registered in three positions of the cutting tool on the workpiece and for different shaft diameters. Both amplitude- and frequency-dependent AE and VA characteristics were obtained and analyzed for overall process signal length as well as for single frames. It was shown that power spectrum characteristic could be used for monitoring the fast-occurring changes in the cutting process stability. A criterion of the cutting process stability based on the power spectrum has been offered.

1 Introduction

Application of peakless cutting tools in machining allows achieving higher precision and quality of processed surfaces [1–3]. In some cases, it becomes even possible to achieve a roughness level comparable to that of fine grinding. At the same time, peakless tool machining is prone to chatter cutting mode, which is an undesirable factor for providing both

surface quality and machining precision. In addition, the vibrations may cause enhanced wear of cutting tools. In order to avoid the vibrations during peakless tool machining, it is reasonable to detect a moment of time when transition from steady to chatter cutting has started. Such an approach implies acquisition and analysis of the real-time signals obtained from a sensor so that either cutting process parameters or the worn tool could be timely changed before the full-scale chatter cutting is established. The cutting process monitoring is feasible with the use of many transducers such as accelerometers, acoustic emission (AE) sensors, strain gauges, microphones, and eddy current coils. The most widely used ones are accelerometers and AE sensors because of their low cost and easy handling.

Main AE sources in metal cutting are as follows: plastic deformation in chip separation, tool/workpiece friction, chip impacting against the tool, tool's edge failure, and elemental chip breaking. Basically, the AE signals are distinguished between continuous and burst ones [4–7]. Earlier studies helped establish a relationship between the AE signals and cutting parameters such as cutting speed or strain rate within the chip formation zone as well as the tool's wear and failure [8–18].

It was shown [6, 19–21] that both cutting tool wear and vibrations generated during the cutting determine the dynamic behavior of the mechanical system. The vibrations have effect on contacting at the tool/workpiece interface so that both real contact area size and the cut layer thickness dynamically vary during cutting and thus change the deformation conditions and AE signal generation in the chip formation zone [6, 21, 22].

The use of both AE and vibration acceleration (VA) sensors seems a promising approach for monitoring various mechanical processes. The vibration acceleration signal is intuitively simple and requires minimal treatment before analyzing it. On the other hand, the AE signal is sensitive to the microscopic-

✉ A. V. Filippov
andrey.v.filippov@yandex.ru

[1] Institute of Strength Physics and Materials Science SB RAS, per. Academicheskii 2/4, Tomsk, Russia

[2] Tomsk Polytechnic University, Lenina av. 30, Tomsk, Russia

Fig. 1 Shear strain localization zones in cutting and chip formation
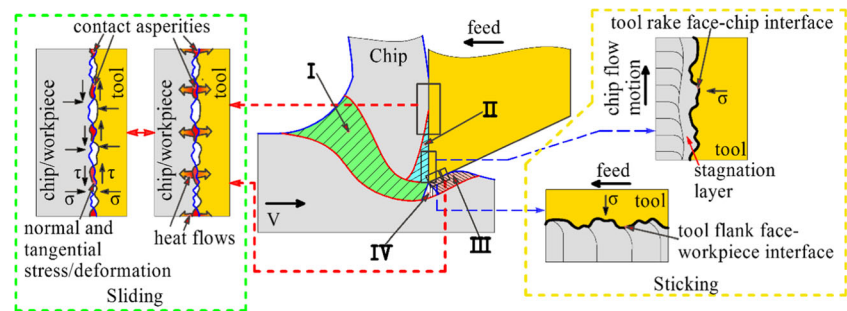
level events and therefore could be effective for detecting the incipient defects. For example, the AE signal was shown to be more effective for condition monitoring on gearboxes and ball bearings and for detecting the defects as compared to the vibration analysis [23–26]. Also, the efficiency of AE monitoring on ball bearings was reported for different working conditions [27–36].

It was noted also [37] that extending the frequency range of monitoring due to combined acquisition of both AE and vibration signals allowed for higher sensitivity of detecting defects in gear wheels.

Both AE and vibration acceleration signals are generated and then changed dynamically during the metal cutting. The AE high-frequency signal is responsible for microscopic-scale friction, deformation, and fracture events while the low-frequency vibration acceleration signal denotes the macroscopic events relating to the entire mechanical system. Analyzing both of them allows better understanding of dynamic processes, which develop in the process of metal cutting.

Metal cutting could be considered as a combination of two processes such as (1) cutting edge penetration into a workpiece and (2) sliding on the workpiece/tool interfaces. According to the insights reported [38–43], three shear strain localization zones could be formed in the cutting process. The primary shear deformation zone *I* is a volume of metal with either homogeneously or inhomogeneously distributed shear strain [44, 45] and where the heat is released due to severe plastic deformation (Fig. 1). The secondary deformation zone *II* is adjoining both the tool's rake face and primary shear zone; in other words, it is a zone where the chip is contacting

the rake face. The chip/rake contact length is characterized by the presence of both sliding and sticking zones (Fig. 1).

The tertiary shear zone *III* is adjoining both flank face and primary shear zone. Also, there is a transition zone between the tertiary and primary zones. The chip/flank face contact length may contain both sticking and sliding zones too.

The sticking and sliding zones' lengths may vary depending upon the cutting conditions such as tool and workpiece materials, cutting mode, and cooling [46–48]. The heat is generated in the secondary and tertiary zones both due to shear deformation and friction.

When the chip sticks to the rake face, it may form an intermediate stagnation (tribological) layer (Fig. 1) which may cover the rake face so that sliding is really at the interface between the chip and this layer. The chip experiences resistance to sliding as determined by the shear stress needed to overcome its cohesion to this layer. According to [49], the sticking provides high contact stress and almost zero sliding speed, which results in forming adhesion bonds at both workpiece/flank and chip/rake faces.

The sliding zone is characterized by a discontinuous contacting mode when the chip and/or workpiece contacts the tool faces only by asperities so that heat is released only within the real contact areas in the form of near-melting temperature flashes [50].

The above-described processes serve as the AE signal sources and could be sensitive to the vibrations imposed. The objective of this paper is to study the relationship between the AE and the vibration acceleration signal in peakless tool turning on the different stiffness shafts and develop a AE criterion for early detection of the chatter mode.

Fig. 2 Scheme of peakless tool cutting test on a slender shaft
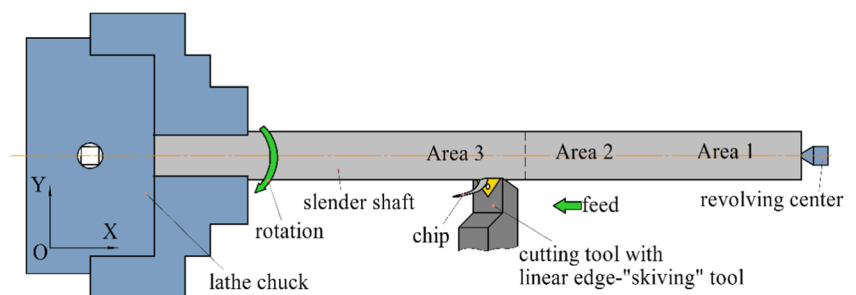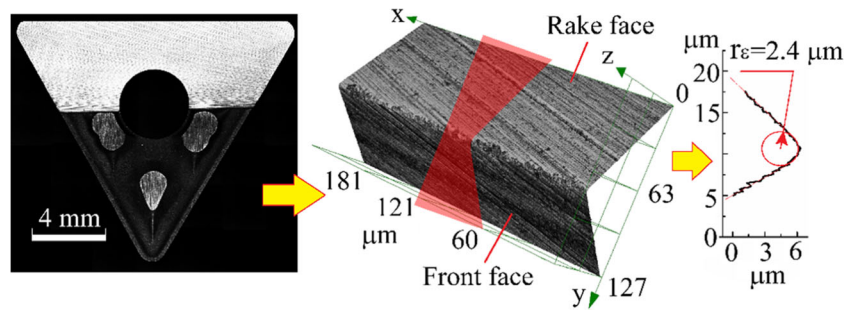
2 Materials and methods

Slender 30 ± 0.05-, 22 ± 0.05-, and 18 ± 0.05-mm-diameter, 300-mm-length shafts made of medium carbon steel AISI 1045 were turned using a lathe machine Okuma ES-L8II-M. Since those shafts had different stiffness, they demonstrated different magnitudes of deflection under mechanical loading from the cutting force depending on the tool position (Fig. 2).

Such an approach has been chosen to simulate the tool working conditions as follows: (a) steady cutting, (b) slow, and (c) fast transition from steady to chatter cutting. Before testing, all shafts have been ground to provide the required diameter accuracy along the shaft's length. All shafts have been fixed in a lathe chuck with the other end supported using a revolving center. Cutting speed was 100 m/min, feed 0.11 mm/rev, and depth of cut 0.3 mm. A rectilinear cutting-edge lathe tool made of ultrafine grain WC-6Co-2TaC hard metal was used for turning (Fig. 3).

Vibration acceleration signals were registered using an IMI industrial accelerometer and USB National Instruments NI-9234 data logger at sampling rate 25.6 kHz.

Acoustic emission signals were registered using an EYa-2 setup developed at Togliatti State University. The AE signal was received by a MSAE-L2 30–1000-kHz bandpass 20-mm-diameter sensor. A low-pass LC filter was used to cut off the < 50-kHz signals generated by the mechanical system components. The AE signals have been reconstructed in the form of either AE signal envelope obtained at a 1-kHz sampling rate and thusly represented the slow-occurring processes, or AE frames recorded at sampling rate 6.25 MHz which

characterized the fast-occurring ones. The recorded frame duration was 0.021 s.

The AE frames have been analyzed together with simultaneously obtained vibration accelerations to investigate the cutting process chatter stability under steady cutting, transition to chatter, and established chatter mode. It is common to study the AE signals by applying the fast Fourier transformation (FFT) and thus obtaining the spectral frequency-domain characteristics such as, for example, median frequency (MF) and power spectrum (PS), which serve to identify the AE signal behavior caused by varying the monitored process parameters. Special software has been developed for determining both mean median frequency and power spectrum values for each frame using the short-time Fourier transformation (STFT) with a rectangle, 1000 × 1000-data point-size window and 300-point-length shift. In doing so, the time dependencies of these characteristics have been reconstructed for the full signal duration.

The VA signal dynamics was assessed using the running root mean square (runRMS) values determined at sampling rate 1 Hz. The amplitude-frequency characteristics have been obtained by means of FFT using the software package Origin 8.6 Pro.

Schematics of the peakless rectilinear edge tool turning experiment are shown in Fig. 2. Three areas of interest on the slender shaft surface are denoted as *area 1*, *area 2*, and *area 3*. The peakless tool was fed starting from *area 1* to *area 3*, thus increasing the slender shaft deflection and therefore the chatter mark risk. The surface roughness of the processed
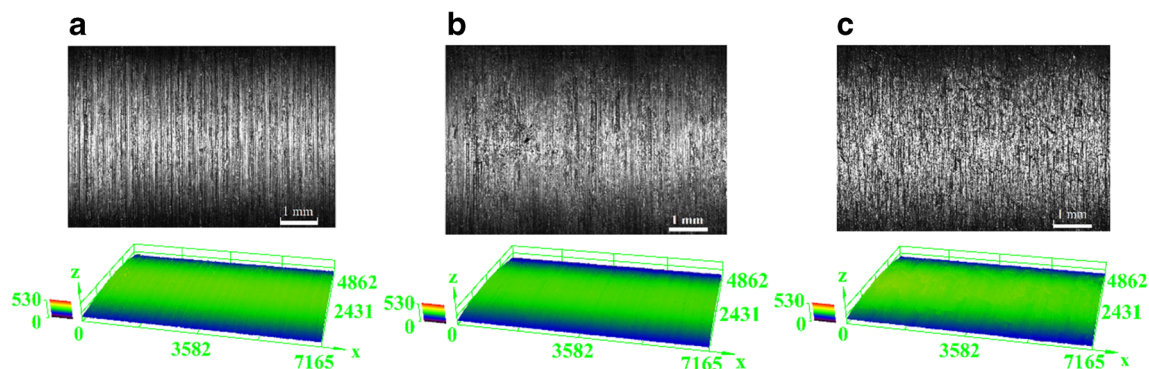
Fig. 4 The 30-mm-diameter shaft surface after steady cutting test from area 1 (**a**), area 2 (**b**), and area 3 (**c**)
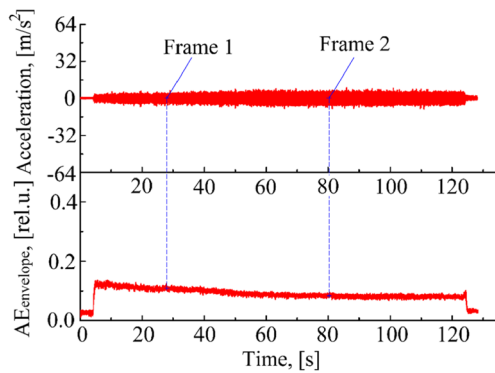
Fig. 5 Acceleration and AE signal envelope registered on test with normal cutting condition

shaft was measured using laser scanning microscope Olympus LEXT OLS4100.

Cutting inserts were sharpened by both rake and flank faces using diamond wheels to provide surface roughness Sa ~ 0.075 μm and cutting edge rounding radius R ~ 2.4 μm (Fig. 3).

3 Results

3.1 Steady turning mode on a 30-mm-diameter shaft

Turning on a 30-mm-diameter shaft was the most stable process which gave surfaces with roughness parameters Sa = 2 μm for areas 1 and 2 and Sa = 3 μm for area 3 (Fig. 1). No waviness or surface corrugation was noticed on the processed surface zones (Fig. 4).

Both AE envelope and vibration acceleration signals demonstrate their stable behavior in time without any bursts (Fig. 5). A detailed study of both signals' behavior has been carried out by obtaining the time dependencies of vibration acceleration runRMS and power spectrum mean values and comparing them to those of AE signal median frequency and power spectrum (Fig. 6). Both MF and PS values were in the ranges 57 to 77 kHz and 1.7×10^{11} to 5.7×10^{11}, respectively. Those signal levels corresponded to the steady cutting mode without any notable shaft vibrations.
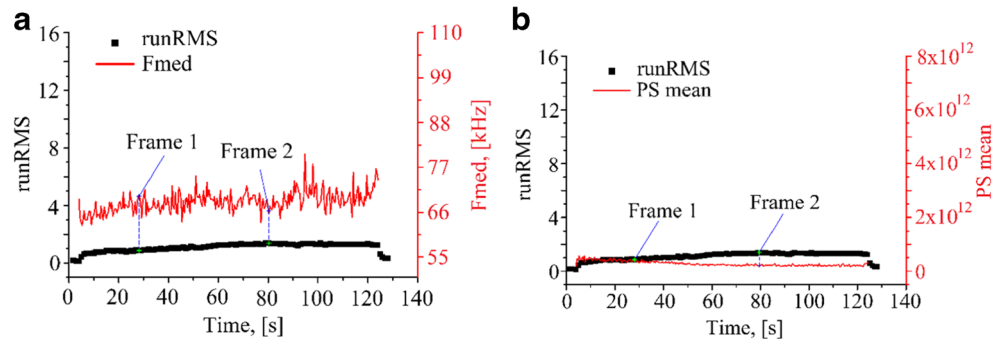
3.1.1 Frame analysis

Acoustic signal emission is a fast-occurring process in distinction to the vibrations. Therefore, it is not a trivial task to compare them. The AE signal contains much more information about the process, and therefore, it is reasonable to make an attempt of getting useful information not only from treating the long-time signal but also from treating the short-time AE signal frame structure. Short-time AE signal and vibration acceleration (VA) frames are shown in Fig. 7. These frames have been selected as shown by lines in Fig. 5 to represent the structure of the cutting process steady stage. It is observable that the AE signal magnitudes are almost the same level with only minor low magnitude bursts (Fig. 7a). The same pattern is observed in case of vibration accelerations (Fig. 7b).
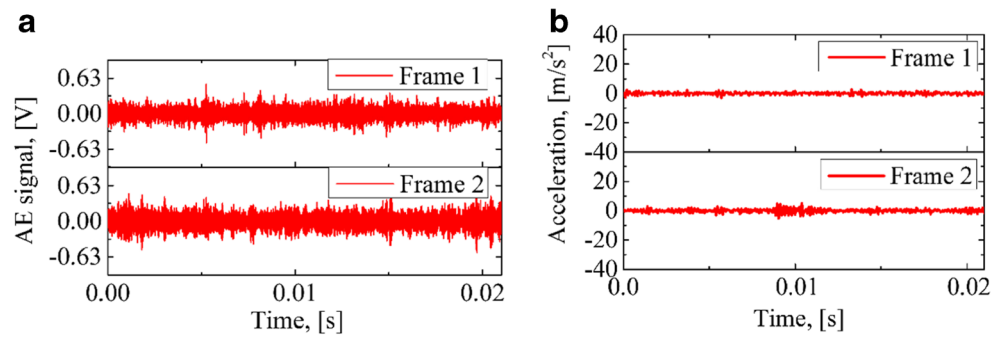
The AE signal median frequency and power spectrum dependencies for two frames obtained during steady turning show that maximum 125-kHz MF peaks are uniformly distributed inside the frames whereas the PS has maximum magnitude 3.7×10^{14} at ~ 60 kHz (Fig. 8a, b). The vibration acceleration magnitude shows some tiny peaks at 7 and 5 kHz for frame 1 and frame 2, respectively (Fig. 8c).

## 3.2 Slow transition to chatter cutting on a 22-mm-diameter shaft

Three typical surface areas can be observed on a 22-mm-diameter shaft after turning (Fig. 9). Area 1 is characterized by small roughness Sa ~ 2.2 μm. Area 2 and area 3 roughness is Sa ~ 3.5 and Sa ~ 5 μm, respectively. In addition, areas 2 and 3 show the surface chatter marks resulting from turning under conditions of vibration. The steady turning stage time was 45 s (Fig. 10) before vibration acceleration magnitude increased slowly. The acceleration magnitude rise time was 25 s. Another type of behavior has been discovered for the AE signal magnitude (Fig. 10). The transition from steady turning to chatter was characterized by a AE signal magnitude fall followed by a rise coinciding in time with that of vibration acceleration magnitude. Also, one can see that the AE signal amplitude experiences low-frequency modulations during the

Fig. 6 Signal parameters on test with normal cutting condition. **a** Acceleration runRMS and mean value of F_{med}. **b** Acceleration runRMS and mean value of PS intensity

Fig. 7 AE (**a**) and VA (**b**) frames in steady cutting mode

Fig. 8 AE signal mean median frequency (**a**), AE signal power spectrum (**b**), and VA amplitude-frequency response (**c**) during steady cutting
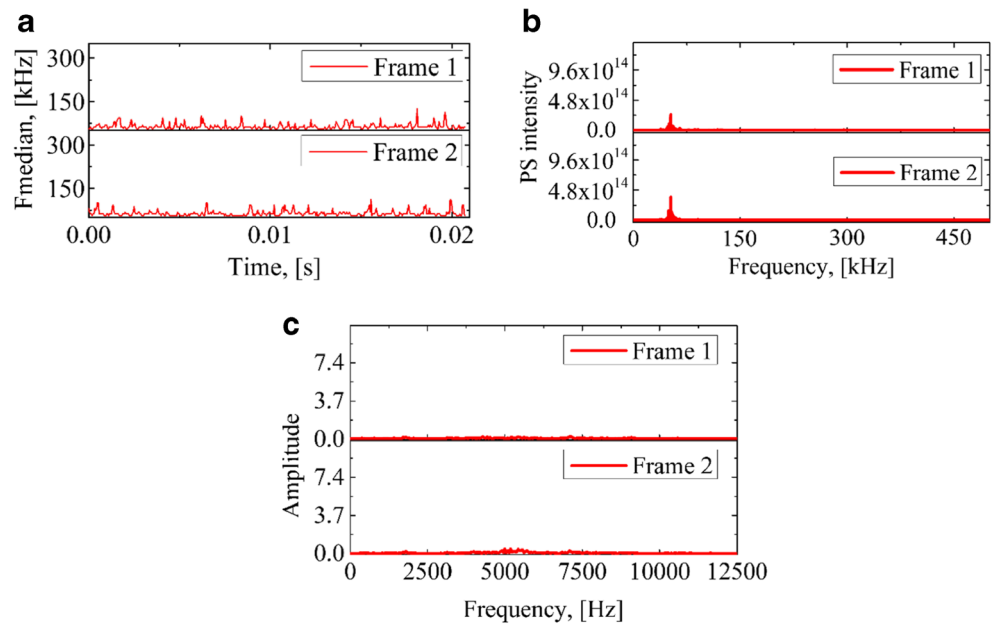
chatter stage which allow suggesting a relationship between AE and VA signal amplitudes.

The AE signal MF behavior in the transition stage is shown in Fig. 11. Comparing Fig. 11 and Fig. 10, one can see that the AE signal falls at the 57th second (Fig. 10) corresponding to the MF rise in Fig. 11a and vice versa, and the AE and VA magnitude rise (Fig. 10) corresponds to the MF fall in Fig. 11a. The AE signal power spectrum magnitude rise coincides with that of vibration acceleration (Fig. 11b). The slow steady/chatter transition stage is characterized by AE signal MF and PS in the range 57 to 106 kHz and 1.5×10^{11}–6×10^{12}, respectively.

3.2.1 Frame analysis

The AE signal as well as vibration acceleration frames 1–2, 3–4, and 5–6 (Fig. 11a, b) have been selected to

Fig. 9 The 22-mm-diameter shaft surface before area 1 (**a**), during area 2 (**b**), and after transition to chatter area 3 (**c**)
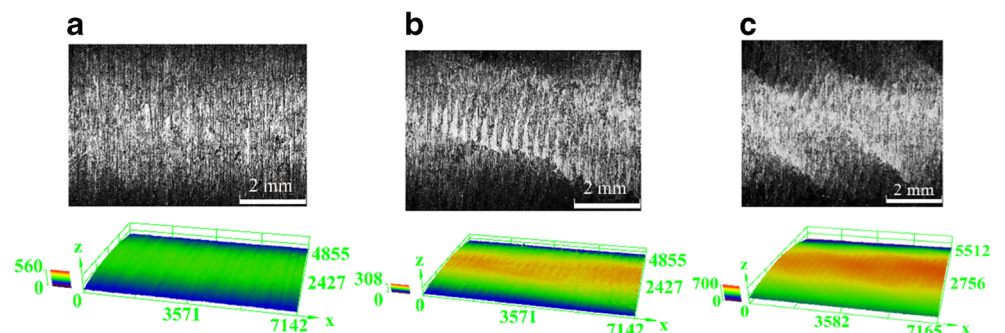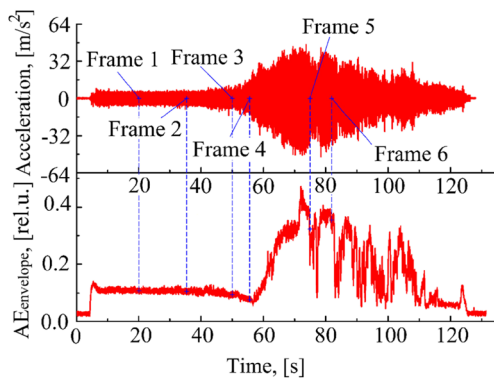
Fig. 10 Acceleration and AE signal envelope registered during the slow low/high-vibration transition cutting test

signal MF peaks for frames 3–4 are at the level of 225 and 300 kHz, respectively. The PS magnitude is reduced to 1.4×10^{13} in the process. The VA shows some growth as follows: 0.57 at 5.1 kHz and 2.43 at 5.43 kHz for frames 3 and 4, respectively. The high-magnitude VA stage demonstrates reduced MF 200–170 kHz but higher 1.2×10^{15} PS magnitude as compared to those of larger-diameter shafts. The VA amplitude reaches its maximum values 9.9 at 5.3 kHz and 10.8 at 5.3 kHz for frames 3 and 4, respectively.

The steady turning mode is characterized by numerous low MF bursts and small number of high MF ones. In transition to chatter turning, the MF shows some

Fig. 11 The AE and VA signals' parameters in the slow low/high-vibration transition mode cutting test. **a** Acceleration runRMS and mean value of F_{median}. **b** Acceleration runRMS and mean value of PS intensity
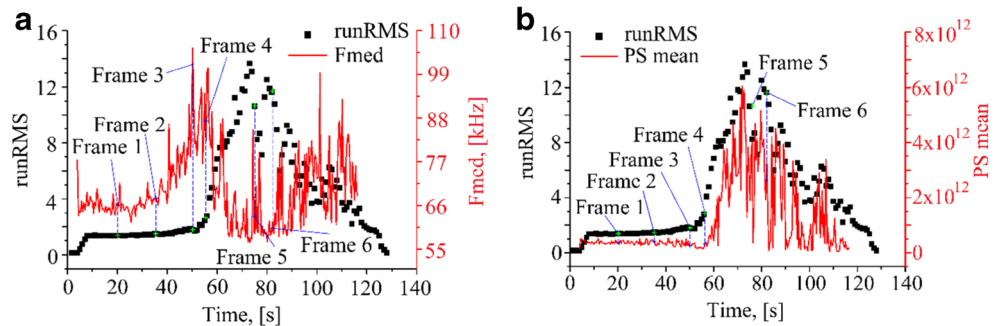

characterize steady cutting and slow and fast transition to chatter, respectively. Frames 1–2 give the waveforms similar to those shown in Fig. 12a, b for the steady cutting stage. Frames 3–4 show both AE and VA bursts whose numbers are increased in transition to the high-magnitude chatter inherent to frames 5–6.

The AE frame MF and PS dependencies in Fig. 13a, b show that frames 1 and 2 possess maximum 115-kHz MF peaks and PS magnitude 3×10^{14} for frequencies below 75 kHz. The VA amplitudes reach 0.7 at ~ 5.5 kHz and 0.5 at ~ 5.3 kHz for frames 1 and 2, respectively. The AE

high-frequency peaks whose number is decreased when approaching the chatter stage (Fig. 13, frame 4). At high VA stage, there are only a couple of MF peaks.

The MF and PS behavior during the transition stage (Fig. 13a, b, frames 3 and 4) allows suggesting that these AE signal parameters are sensitive to the process mode changes. The corresponding AE frames reveal high MF and low, almost zero-level PS. At the same time, VA (Fig. 13c) demonstrates only a minor amplitude growth. Such a fact allows suggesting that there is an interval where high-frequency AE noise is induced by onset low-

Fig. 12 The AE (**a**) and VA (**b**) frames in slow transition to the chatter cutting test
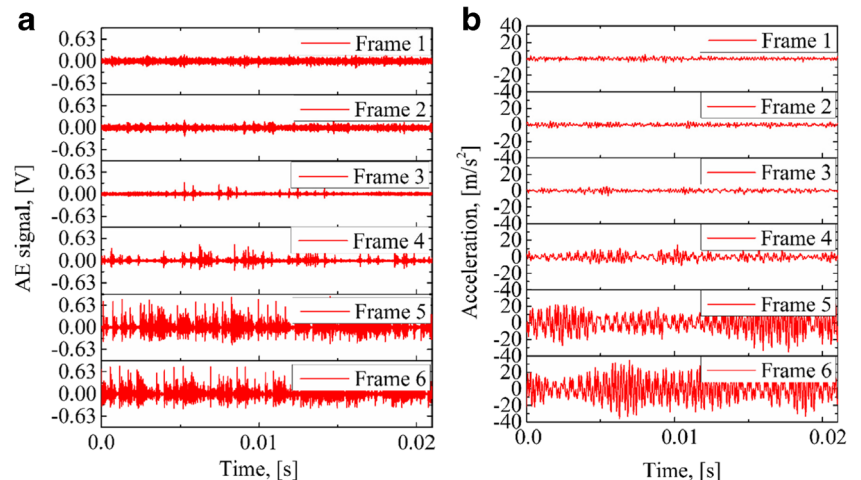
Fig. 13 AE signal mean median frequency (**a**), AE signal power spectrum (**b**), and VA amplitude-frequency response (**c**) during the slow low/high-vibration transition mode cutting test
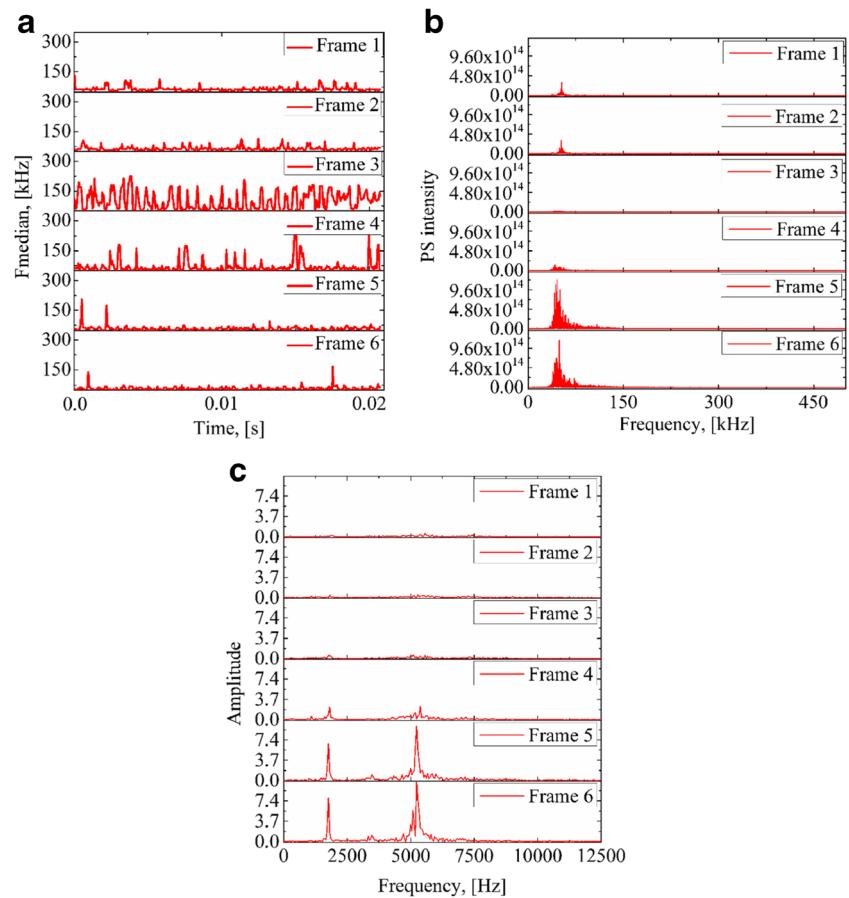
amplitude VA oscillations. The AE signal energy is almost uniformly distributed along the frequency axis in this case. Also, one can suggest that these high-frequency AE signals might reduce the cutting force similar to when it occurs in vibration-assisted machining (VAM). Further VA amplitude growth results in PS peak at about 60 kHz, i.e., the same as in steady cutting mode (frames 1 and 2).

### 3.3 Fast transition to chatter cutting on an 18-mm-diameter shaft

The shaft surface roughness increased to Sa ~ 4.3 μm, Sa ~ 6.5 μm, and Sa ~ 6.6 μm for area 1, area 2, and area 3,

respectively (Fig. 14). The chatter marks in this case are present in all the shaft's surface areas. Steady vibration-free turning stage on the 18-mm-diameter shaft lasts only for the first 5–7 s being followed by fast transition to high VA magnitude chatter (Fig. 15). The transition was accompanied by a synchronous AE signal magnitude growth.

The AE signal frames as those indicated in Fig. 15 have been chosen for reconstructing the MF and PS time dependencies shown in Fig. 16. The steady turning stage was too short and represented by only two frames 1 and 2 in Fig. 15 where we still can see that transition to high-magnitude VA chatter was accompanied by a decrease in

Fig. 14 The 18-mm-diameter shaft surface before area 1 (**a**), during area 2 (**b**), and after transition to chatter area 3 (**c**)
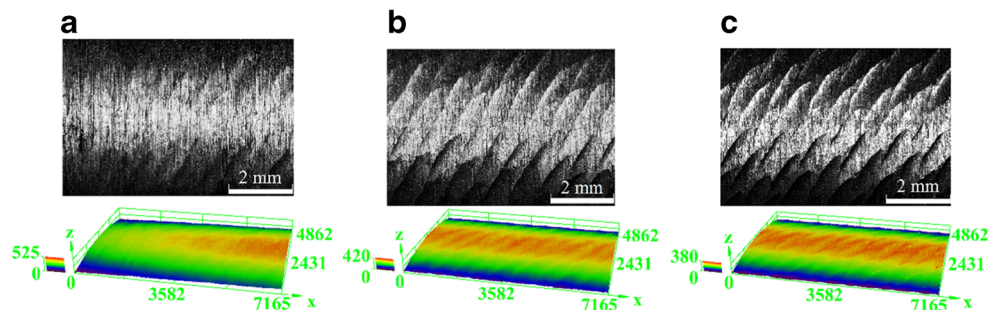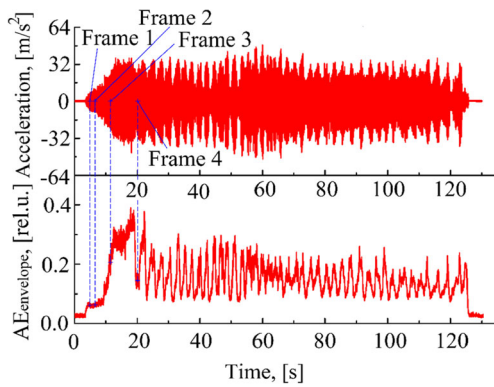
Fig. 15 Acceleration and AE signal envelope registered during the fast low/high-vibration transition test

signals under steady cutting mode show almost no bursts except for several ones in frame 2 (Fig. 17a). The number of AE signal bursts increased for frame 3 and even more for frame 4. The VA waveforms look similar to those in Fig. 12b.

The maximum MF peaks for frames 1 and 2 are at 150 and 200 kHz, respectively (Fig. 18). The number of the low-frequency peaks is much higher than that of the high-frequency ones. The VA amplitude for frames 1 and 2 is 1.1 at ~ 5.3 kHz and 2.63 at ~ 2 kHz. The VA amplitude is increased in transition to the chatter turning and

Fig. 16 Signal parameters on fast low/high vibration transition test. **a** Acceleration runRMS and mean value of F_{median}. **b** Acceleration runRMS and mean value of PS intensity
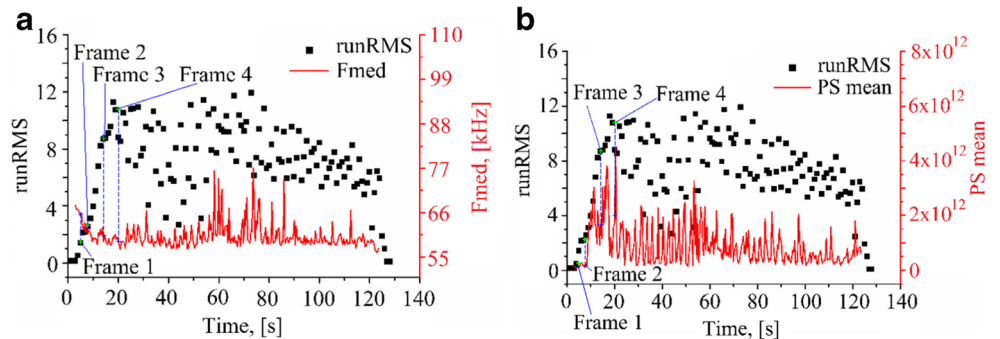
the MF and increase in the PS magnitudes (Fig. 16a, b). The fast transition stage is characterized by AE signal MF and PS in the range 56 to 77 kHz and 1.1×10^1 to 4.5×10^{12}, respectively.

3.3.1 Frame analysis

In case of fast transition to chatter cutting, frames 1–2, 3, and 4 corresponded to short-time steady stage, transition, and high VA magnitude chatter, respectively. The AE

achieves 5.31 at 2 kHz for frame 3. The high-magnitude stage results in VA level 10.1 at 5.6 kHz. The PS magnitude grows starting from the steady mode value ~ 4×10^{13} to the high-magnitude ~ 4×10^{14}.

Steady turning mode is characterized by a large number of low-frequency peaks and only few high-frequency ones. A number of low-frequency MF peaks is typical for transition to the chatter stage (frame 3). High-magnitude VA chatter mode (frame 4) produced only a couple of high-frequency MF peaks.

Fig. 17 AE (**a**) and VA (**b**) frames in the fast low/high-vibration transition mode cutting test
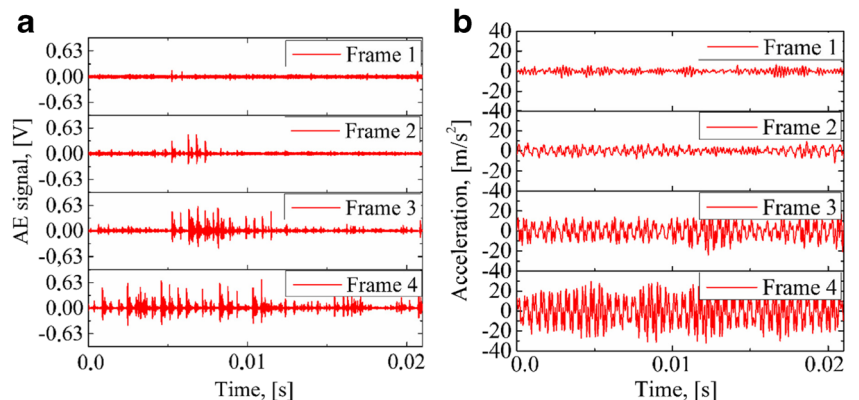
Fig. 18 AE signal mean median frequency (**a**), AE signal power spectrum (**b**), and VA amplitude-frequency response (**c**) during the fast low/high-vibration transition mode cutting test

Fig. 19 Oscillation mode in turning on a low stiffness shaft
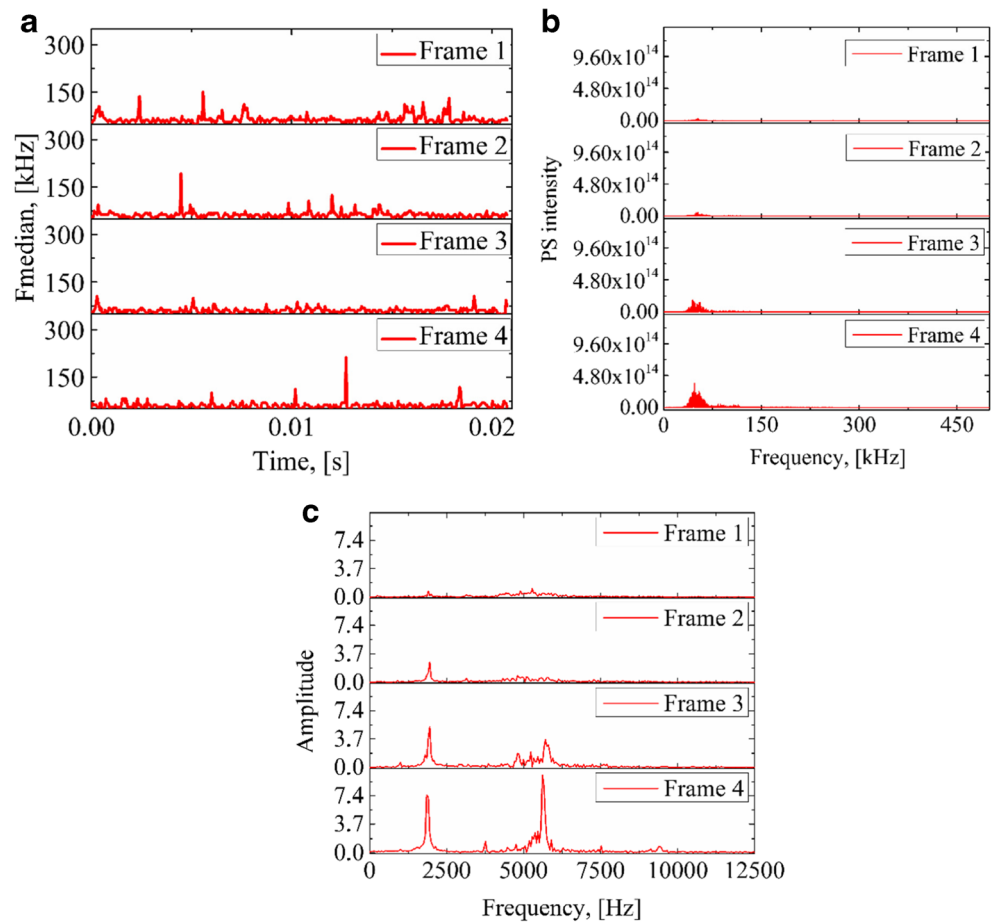
4 Discussion

The results of experiments show that there is a relationship between AE and VA signals in machining on the workpieces having different levels of stiffness. First of all, the AE amplitude simultaneously grows together with that of VA. The AE signal mean median frequency dependence on time shows that MF is decreased during chatter cutting while the power spectrum behavior coincides in time with that of the VA runRMS/frequency. Third, the crossover from steady to chatter machining is characterized first by increasing the mean MF and decreasing it for higher VA runRMS amplitudes. When reaching its maximum value, the run RMS begins to decrease along with a simultaneous decrease in the AE signal mean MF.

A detailed study of these effects was undertaken with the use of single frame structure. Frames typical for the AE and VA signal behavior have been studied following the procedure the same as for full waveforms.

It was established that the mean characteristics reflect the inner structure of AE frames with respect to median frequency, power spectrum, and VA amplitude-frequency response. Let us dwell on the specificity of machining and AE signal generation with respect to slender shafts.

Turning on slender shafts may be accompanied by oscillations due to low stiffness of the workpiece/tool system. These oscillations will be generated mainly by the workpiece under condition of low enough cutting depth. The reason for oscillations is the elastic radial Δy and tangential Δz deflections resulting from the corresponding cutting force components Py and Pz (Fig. 19). In its turn, deflection is the reason for the cutting depth variations during turning which are the reason for corrugating the workpiece's surface. The smaller is the
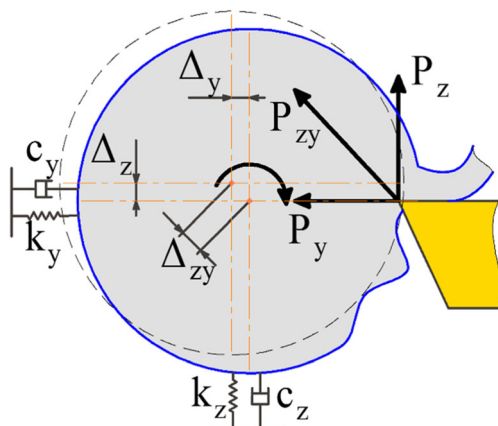
Fig. 20 The contact length and cut layer thickness changes during turning on the oscillating workpiece
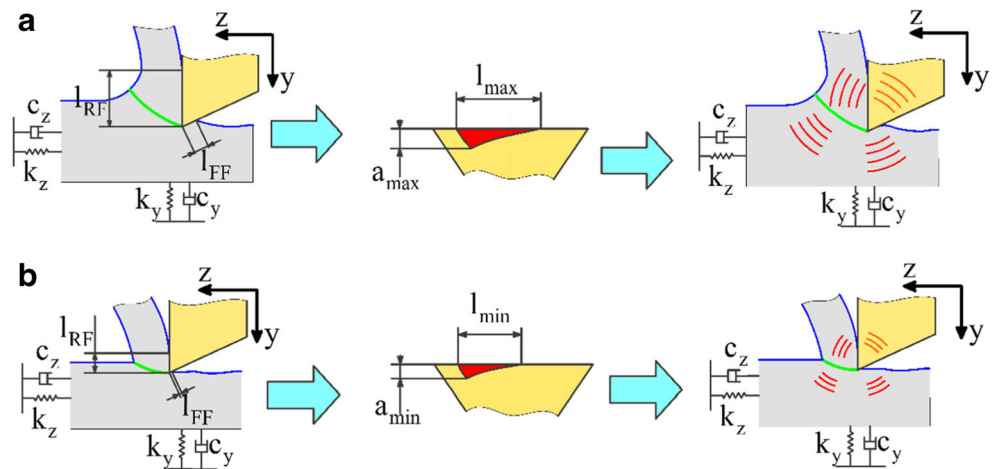
workpiece diameter, the higher is the deflection magnitude, the workpiece length kept constant.

Let us see that in more detail by the example of pointless rectilinear edge tool turning. In such a situation, the elastic deflections (Fig. 19) may change the rake and flank face contact length L_{RF} and L_{FF} as well as both maximum width l_{max} and maximum thickness a_{max} of a layer cut (Fig. 20). The notable instability of the cut layer thickness then results in change in the chip formation conditions all the way to a discontinuous chip formation (Fig. 20). This is an explanation for the chatter marks on the shaft areas during the chatter stage of turning.

Let us look at an effect that vibrations may produce on the interface between the tool and the workpiece (Fig. 21, states 1–3). The vibrations may cause both surface separation *state 2* and surface proximity *state 3* due to vertical vibration displacements. The proximity will provide

higher compression strain and real contact surface area between the workpiece and the rake/flank tool's faces. Horizontal vibration displacements will produce shear strain beneath the workpiece's real contact areas which then may result in stick-slip mode sliding as shown by *state 4*. The latter may be the sources of the AE signal bursts observed during transition to chatter turning mode as shown by *state 5*.

It was established that the behavior of AE mean power spectrum value in time correlates with that of VA runRMS (Fig. 11b). It was shown above (see Fig. 8b) that the mean PS level was minimal during the steady cutting mode. Transition to chatter mode cutting was accompanied by appearing mean PS peaks and valleys (Figs. 13b and 18b). Such a correlation allowed us to propose the AE power spectrum mean variance value as a criterion for describing the turning process stability.

Fig. 21 Effect of vibrations on the AE signal generation
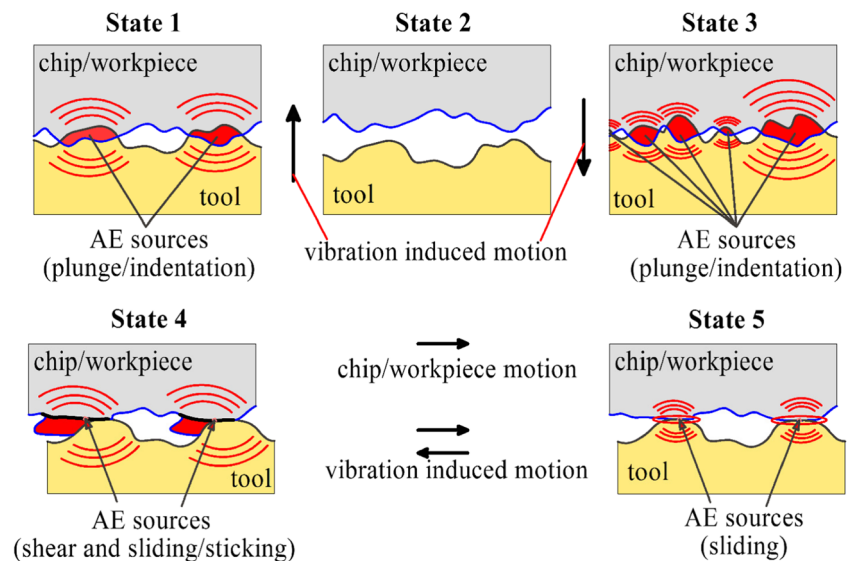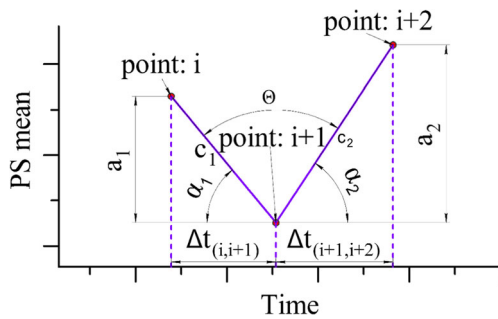
Fig. 22 Towards determining the AE PS variance Θ

This criterion may be denoted as an angle Θ between two lines drawn to connect three successive PS points i, i + 1, and i + 2 (Fig. 22).

The angle Θ magnitude is determined by equations as follows:

$$\Theta = 180° - (\alpha_1 + \alpha_2),$$
$$\alpha_1 = \sin\left(\frac{|PS_i - PS_{i+1}|}{\sqrt{(PS_i - PS_{i+1}) + (\Delta t_{i,i+1})^2}}\right),$$
$$\alpha_2 = \sin\left(\frac{|PS_{i+1} - PS_{i+2}|}{\sqrt{(PS_{i+1} - PS_{i+2}) + (\Delta t_{i+1,i+2})^2}}\right).$$

where PS_i, PS_{i+1}, and PS_{i+2} are normalized PS magnitudes in points i, i + 1, and i + 2, respectively.

Δt_i, Δt_{i+1}, and Δt_{i+2} are the time intervals between successive frames i, i + 1, and i + 2, respectively.

The PS-normalized magnitude is obtained by dividing the frame mean PS by the maximum first-frame PS value. One of the advantages offered by such an approach relates to the calculation procedure which allows dealing with only a 0.02-s-duration frame instead of treating the full AE signal waveform. Therefore, we can obtain a prompt response from the mechanical system which is important for the purpose of monitoring the cutting chatter stability.

The AE PS variance time dependence for steady cutting mode is shown in Fig. 23 in comparison to that of VA
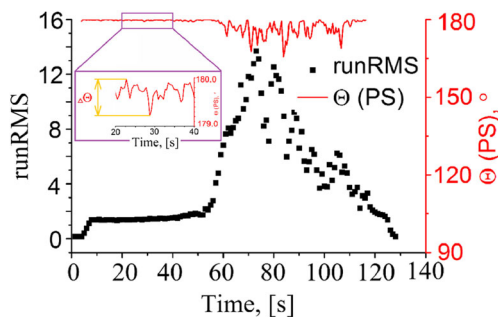
runRMS. It is seen that $\Delta\Theta$ is not above 1° in this case. Under condition of transition to chatter cutting and severe chatter, $\Delta\Theta$ becomes one order magnitude higher, i.e., 10° and 15°, respectively.

In case of turning on an 18-mm-diameter shaft with fast transition to chatter, the AE PS variance $\Delta\Theta$ for very short steady cutting, fast transition, and severe chatter mode is 1°, 10°, and 20°, respectively (Fig. 24).

5 Conclusions

A peakless tool turning process on slender shaft workpieces has been used to simulate the dynamic transition from steady to chatter mode cutting and study the system acoustic emission and vibration acceleration responses. The cutting process conditions have been characterized by the AE signal median frequency and power spectrum. For steady cutting, the MF dependency on time shows a number of low-frequency peaks with several high-frequency ones. More high-frequency MF peaks appear in transition to the chatter mode caused by turning on a lower stiffness 22-mm-diameter shaft. The chatter mode again shows the smaller number of the high-frequency MF peaks.

It was shown that both AE signal median frequency and power spectrum values are sensitive to the dynamic behavior of the turning process system in contrast to the vibration acceleration frame analysis whose amplitude-frequency dependence shows a monotonous growth only in transition from a steady to chatter mode cutting. The VA amplitude growth is accompanied by synchronous changes of the AE signal mean PS magnitude. In connection with that, we offer a criterion for estimating the turning process stability. This criterion is the AE signal PS variance Θ which may be determined even for isolated short 0.02-s-duration AE signal frames and thus allow the real-time monitoring of the process state. The physical explanation of the experimentally discovered fact that the AE signal spectral characteristics change under chatter mode may be provided from considering the full system energy redistribution depending on the vibrations imposed. It was

Fig. 23 The AE PS variance angle Θ for slow transition to chatter mode and severe chatter mode
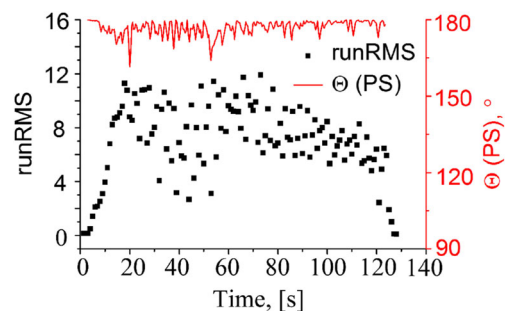
Fig. 24 The AE PS variance angle Θ for fast transition to chatter mode and severe chatter mode

shown [51] with the use of molecular dynamics modeling that the full system energy grows under chatter mode mainly at the account of its potential energy component so that more and more atoms become involved in deformation and therefore spectral characteristics of the system are changed.

References

1. Grzesik W, Zak K (2012) Surface integrity generated by oblique machining of steel and iron parts. J Mater Process Technol 212: 2586–2596. https://doi.org/10.1016/j.jmatprotec.2012.07.019
2. Grzesik W (1986) Stereometric and kinematic problems occurring during cutting with single-edged tools. Int J Mach Tools Manuf 26: 443–457. https://doi.org/10.1016/0020-7357(86)90034-X
3. Monka P, Monkova K, Balara M, Hloch S, Rehor J, Andrej A, Somsak M (2016) Design and experimental study of turning tools with linear cutting edges and comparison to commercial tools. Int J Adv Manuf Technol 85:2325–2343. https://doi.org/10.1007/s00170-015-8065-3
4. Li X (2002) A brief review: Acoustic emission method for tool wear monitoring during turning. Int J Mach Tools Manuf 42:157–165. https://doi.org/10.1016/S0890-6955(01)00108-0.
5. Inasaki I (1998) Application of acoustic emission sensor for monitoring machining processes. Ultrasonics 36:273–281. https://doi.org/10.1016/S0041-624X(97)00052-8
6. Chiou RY, Liang SY (2000) Analysis of acoustic emission in chatter vibration with tool wear effect in turning. Int J Mach Tools Manuf 40:927–941. https://doi.org/10.1016/S0890-6955(99)00093-0
7. Moriwaki T, Okushima K (1980) Detection for cutting tool fracture by acoustic emission measurement. CIRP Ann-Manuf Technol 29: 35–40. https://doi.org/10.1016/S0007-8506(07)61291-8
8. Dornfeld D (1992) Application of acoustic emission techniques in manufacturing. NDT E Int 25:259–269. https://doi.org/10.1016/0963-8695(92)90636-U
9. Kannatey-Asibu E, Dornfeld D a (1981) Quantitative relationships for acoustic emission from orthogonal metal cutting. J Eng Ind 103: 330. https://doi.org/10.1115/1.3184493
10. Kannatey-Asibu E, Dornfeld DA (1982) A study of tool wear using statistical analysis of metal-cutting acoustic emission. Wear 76: 247–261. https://doi.org/10.1016/0043-1648(82)90009-6
11. Teti R, Dornfeld D (1989) Modeling and experimental analysis of acoustic emission from metal cutting. J Eng Ind 111:229–237. https://doi.org/10.1115/1.3188754
12. Iwata K, Moriwaki T (1977) An application of acoustic emission measurement to in-process sensing of tool wear. Annals of the CIRP 25(1):21–26
13. Iwata K, Moriwaki T (1978) Cutting state identification and in-process tool wear sensing by acoustic emission, Bulletin of the Japanese Society for. Precis Eng 12:213–215
14. Dornfeld DA, Diei E (1982) Acoustic emission from simple upsetting of solid cylinders. J Eng Mater Technol Trans ASME 104:145–152. https://doi.org/10.1115/1.3225049.
15. Dornfeld DA (1983) Investigation of metal cutting and forming process fundamentals and control using acoustic emission, in: Proceedings of the Tenth NSF Conference on Production Research and Technology, Detroit, MI, March 1983
16. Cho SS, Komvopoulos K (1997) Correlation between acoustic emission and wear of multi-layer ceramic coated carbide tools. J Manuf Sci Eng 119(1997):238–246. https://doi.org/10.1115/1.2831100
17. Chiou RY, Liang SY (2000) Dynamic modeling of cutting acoustic emission via piezoelectric actuator wave control. Int J Mach Tools Manuf 40:641–659. https://doi.org/10.1016/S0890-6955(99)00095-4
18. Hase A, Wada M, Koga T, Mishina H (2014) The relationship between acoustic emission signals and cutting phenomena in turning process. Int J Adv Manuf Technol 70:947–955. https://doi.org/10.1007/s00170-013-5335-9
19. Venkata Rao K, Murthy BSN, Mohan Rao N (2013) Cutting tool condition monitoring by analyzing surface roughness, work piece vibration and volume of metal removed for AISI 1040 steel in boring. Meas J Int Meas Confed 46:4075–4084. https://doi.org/10.1016/j.measurement.2013.07.021
20. Subramanian M, Sakthivel M, Sooryaprakash K, Sudhakaran R (2013) Optimization of end mill tool geometry parameters for Al7075-T6 machining operations based on vibration amplitude by response surface methodology. Meas J Int Meas Confed 46:4005–4022. https://doi.org/10.1016/j.measurement.2013.08.015
21. Simeone A, Segreto T, Teti R (2013) Residual stress condition monitoring via sensor fusion in turning of Inconel 718. Procedia CIRP 12:67–72. https://doi.org/10.1016/j.procir.2013.09.013
22. Axinte DA, Gindy N (2003) Tool condition monitoring in broaching. Wear 254:370–382. https://doi.org/10.1016/S0043-1648(03)00003-6
23. Loutas TH, Sotiriades G, Kalaitzoglou I, Kostopoulos V (2009) Condition monitoring of a single-stage gearbox with artificially induced gear cracks utilizing on-line vibration and acoustic emission measurements. Appl Acoust 70:1148–1159. https://doi.org/10.1016/j.apacoust.2009.04.007
24. Al-Ghamd AM, Mba D (2006) A comparative experimental study on the use of acoustic emission and vibration analysis for bearing defect identification and estimation of defect size. Mech Syst Signal Process 20:1537–1571. https://doi.org/10.1016/j.ymssp.2004.10.013
25. Tandon N, Mata S (1999) Detection of defects in gears by acoustic emission measurement. J Acoustic Emission 17(1–2):23–27
26. Singh A, Houser DR, Vijayakar S (1996) Early detection of gear pitting, Power transmission and gearing conference. ASME, DE 88: 673–678
27. Rogers LM (1979) The application of vibration signature analysis and acoustic emission source location to on-line condition monitoring of anti-friction bearings. Tribol Int 12:51–58. https://doi.org/10.1016/0301-679X(79)90001-X
28. Mba D, Bannister RH, Findlay GE (1999) Condition monitoring of low-speed rotating machinery using stress waves Part 1. Proc Inst Mech Eng Part E J Process Mech 213:153–170. https://doi.org/10.1243/0954408991529906
29. Jamaludin N, Mba D, Bannister RH (2001) Condition monitoring of slow-speed rolling element bearings using stress waves. J Process Mech Eng 215:245–271. https://doi.org/10.1243/0954408011530488
30. Yoshioka T, Fujiwara T (1982) New acoustic emission source locating system for the study of rolling contact fatigue. Wear 81(1): 183–186. https://doi.org/10.1016/0043-1648(82)90314-3
31. Yoshioka T, Fujiwara T (1984) Application of acoustic emission technique to detection of rolling bearing failure. Am Soc Mech Eng 14:55–76
32. Hawman MW, Galinaitis WS (1988) Acoustic emission monitoring of rolling element bearings, IEEE 1988 Ultrason. Symp Proc 2: 885–889. https://doi.org/10.1109/ULTSYM.1988.49503
33. Holroyd TJ, Randall N (1993) Use of acoustic emission for machine condition monitoring. Br J Non-Destr Test 35(2):75–78

34. Holroyd T (2001) Condition monitoring of very slowly rotating machinery using AE techniques, 14th International Congress on Condition Monitoring and Diagnostic Engineering Management (COMADEM'2001), Manchester, UK, 4–6 September 2001, 29 (ISBN 0080440363)

35. Bagnoli S, Capitani R, Citti P (May 1988) Comparison of accelerometer and acoustic emission signals as diagnostic tools in assessing bearing. Proceedings of Second International Conference on Condition Monitoring, London, UK, pp 117–125

36. Morhain A, Mba D (2003) Bearing defect diagnosis and acoustic emission. J Eng Tribol 217:275–272. https://doi.org/10.1243/135065003768618614

37. Skrickij V, Bogdevičius M, Junevičius R (2016) Diagnostic features for the condition monitoring of hypoid gear utilizing the wavelet transform. Appl Acoust 106:51–62. https://doi.org/10.1016/j.apacoust.2015.12.018

38. Fang N (2003) Slip-line modeling of machining with a rounded-edge tool—part I: analysis of the size effect and the shear strain-rate. J. Mech. Phys. Solids. 51:715–742. https://doi.org/10.1016/S0022-5096(02)00061-3.

39. Fang N (2003) Slip-line modeling of machining with a rounded-edge tool—part II: analysis of the size effect and the shear strain-rate. J Mech Phys Solids 51:743–762. https://doi.org/10.1016/S0022-5096(02)00061-3.

40. Huang X-D, Zhang X-M, Ding H (2016) A novel relaxation-free analytical method for prediction of residual stress induced by mechanical load during orthogonal machining. Int J Mech Sci 115:299–309. https://doi.org/10.1016/j.ijmecsci.2016.06.024.

41. Budak E, Ozlu E, Bakioglu H, Barzegar Z (2016) Thermo-mechanical modeling of the third deformation zone in machining for prediction of cutting forces. CIRP Ann-Manuf Technol. 8–11.: https://doi.org/10.1016/j.cirp.2016.04.110.

42. Lee S, Hwang J, Shankar MR, Chandrasekar S, Compton W (2006) Large strain deformation field in machining. Metall Mater Trans A 37:1633–1643. https://doi.org/10.1007/s11661-006-0105-z

43. Guo Y, Compton WD, Chandrasekar S (2015) In situ analysis of flow dynamics and deformation fields in cutting and sliding of metals, Proc R Soc A Math Phys Eng Sci 471 doi:https://doi.org/10.1098/rspa.2015.0194.

44. Oxley PLB (1989) The mechanics of machining: an analytical approach to assessing machinability, 1st edn. John Wiley & Sons, New York

45. Kobayashi S, Thomsen EG (1959) Some observations on the shearing process in metal cutting. J Eng Ind 81:251–262

46. Moufki A, Devillez A, Dudzinski D, Molinari A (2004) Thermomechanical modelling of oblique cutting and experimental validation. Int J Mach Tools Manuf 44:971–989. https://doi.org/10.1016/j.ijmachtools.2004.01.018

47. Madhavan V, Chandrasekar S, Farris TN (2002) Direct observations of the chip-tool interface in the low speed cutting of pure metals. J Tribol 124:617. https://doi.org/10.1115/1.1398546

48. Ackroyd B, Chandrasekar S, Compton WD (2003) A model for the contact conditions at the chip-tool interface in machining. J Tribol 125:649. https://doi.org/10.1115/1.1537747

49. Coubron C et al (2013) On the existence of a thermal contact resistance at the tool-chip interface in dry cutting of AISI 1045: formation mechanisms and influence on the cutting process. Appl Thermal Eng 50:1311–1325. https://doi.org/10.1016/j.applthermaleng.2012.06.047

50. Blok H (1963) The flash temperature concept. Wear 6:483–494. https://doi.org/10.1016/0043-1648(63)90283-7.

51. Filippov AV, Nikonov AY, Rubtsov VE, Dmitriev AI, Tarasov SY (2017) Vibration and acoustic emission monitoring the stability of pealess tool turning: experiment and modeling. J Mat Process Tech 246:224–234